Field-Driven Dynamics of Correlated Electrons in LiH and $NaBH_4$ Revealed by Femtosecond X-Ray Diffraction

Vincent Juvé,[1,*] Marcel Holtz,[1] Flavio Zamponi,[1,†] Michael Woerner,[1,‡] Thomas Elsaesser,[1] and A. Borgschulte[2]

[1]*Max-Born-Institut für Nichtlineare Optik und Kurzzeitspektroskopie, 12489 Berlin, Germany*

[2]*Swiss Federal Laboratories for Materials Testing and Research, Laboratory for Hydrogen and Energy, EMPA, CH-8600 Dübendorf, Switzerland*

(Received 18 June 2013; published 19 November 2013)

We study the quasi-instantaneous change of electron density in the unit cells of LiH and $NaBH_4$ in response to a nonresonant strong optical field. We determine for the first time the related transient electron density maps, applying femtosecond x-ray powder diffraction as a structure probe. The light-induced charge relocation in $NaBH_4$ exhibits an electron transfer from the anion (BH_4^-) to the Na^+ cation. In contrast, LiH displays the opposite behavior, i.e., an increase of the ionicity of LiH in the presence of the strong electric field. This behavior originates from strong electron correlations in LiH, as is evident from a comparison with quasiparticle band structures calculated within the Coulomb-hole-plus-screened-exchange formalism.

DOI: 10.1103/PhysRevLett.111.217401 PACS numbers: 78.47.J−, 72.20.Ht, 72.80.Ey, 78.70.Ck

Physical processes driven by external electric fields play a key role for the electronic and optical properties of condensed matter. Nonperturbative interactions with fields of an amplitude comparable to the inner-atomic fields in solids allow for studying new regimes of charge transport such as coherent ballistic electron motions [1] and/or for inducing a highly nonlinear optical response [2]. The latter results in phenomena such as field-driven electron emission [3], interband tunneling [4], high harmonic generation [5], and/or light-driven charge relocations [6]. Recently, intense optical pulses of a few femtosecond duration have been applied to drive charge transport in insulators [7,8].

The electron density $\rho(\mathbf{r}, t)$ in crystalline matter transiently deformed by strong electric fields contains both temporal (or frequency) and spatial (or k-space) aspects. So far, most experimental studies had their focus on the temporal (or frequency) aspects, i.e., on transient macroscopic polarizations and currents [1–8]. The results have given only indirect insight into Coulomb mediated electronic correlations which—in contrast—have been the subject of extensive theoretical work [9–20]. Moreover, the real space dynamics of charges on atomic length scales, which are a probe of electronic correlations, have remained mostly unresolved. Here, ultrafast time-resolved x-ray and electron diffraction experiments can provide direct insight as the structure factors governing transient diffraction patterns are determined by the Fourier transform of the time-dependent spatial electron distribution [21–24]. Following this approach, we have mapped field-driven electron relocations in the ionic material $LiBH_4$ by femtosecond x-ray powder diffraction [25]. In Ref. [6], experiments on a single reflection have been combined with a theory for the transient charge density map $\rho(\mathbf{r}, t)$.

In this Letter, we apply femtosecond x-ray powder diffraction to reveal the field-driven dynamics of correlated electrons in the prototype ionic materials LiH and $NaBH_4$. The simultaneous measurement of intensity changes of different diffraction rings provides the transient structure factors from which we derive spatially resolved electron density maps. LiH is the simplest heteronuclear solid which has been studied in nuclear physics and used in various hydrogen storage systems. According to theory, it should display strong adiabatic [9–20] and nonadiabatic electron correlations [26,27]. We demonstrate for the first time a quasi-instantaneous increase of the ionicity of LiH in the presence of the strong electric field, i.e., a transient electron transfer from the Li to the neighboring H atoms. A comparison with model calculations shows that a mean-field theory, i.e., the Hartree-Fock approximation, fails to account for this behavior. However, calculations including Coulomb correlations on the most basic level, i.e., quasiparticle band structures calculated within the Coulomb-hole-plus-screened-exchange (COHSEX) formalism [14,17], predict correctly the increase of the ionicity of LiH. In contrast, $NaBH_4$ displays a charge transfer from the negative BH_4^- to the Na^+ ions, reducing the ionicity of the material as expected for a predominant admixture of states in the lowest conduction band.

The experiments make use of a femtosecond pump-probe scheme where a nonresonant femtosecond pulse provides the external electric field interacting with the material, and the resulting change in the distribution of electronic charge is monitored by diffracting hard x-ray pulses from the sample which consists of a powder of small crystallites [28]. Both pump and probe pulses are derived from an amplified Ti:sapphire laser system delivering sub-50-fs pulses centered at 800 nm with an energy per pulse of 5 mJ and a repetition rate of 1 kHz. The excitation pulses at 800 nm have a peak amplitude of the electric field of 1 GV/m. The main fraction of the laser output drives a

plasma source [29] providing hard x-ray pulses of a photon energy of 8.06 keV (Cu$K\alpha$) and a duration of approximately 100 fs. Ring patterns of x rays diffracted from the powder samples are detected by a large-area detector (Pilatus Dectris 1M) for different pump-probe delays. The pump beam is mechanically chopped with the 25 Hz readout rate of the detector to improve the signal-to-noise ratio and to determine the absolute changes of diffracted intensity. The powder diffraction pattern on the detector consists of elliptic and hyperbolic rings, each corresponding to one (or several equivalent) set(s) of lattice planes hkl [Fig. 1(a)]. The exposure time per time delay step was set to 140 s, and we collected around 2300 time delay steps for several days with a fresh sample everyday. The all optical autocorrelation was measured repeatedly to assure a proper stacking of the different data sets.

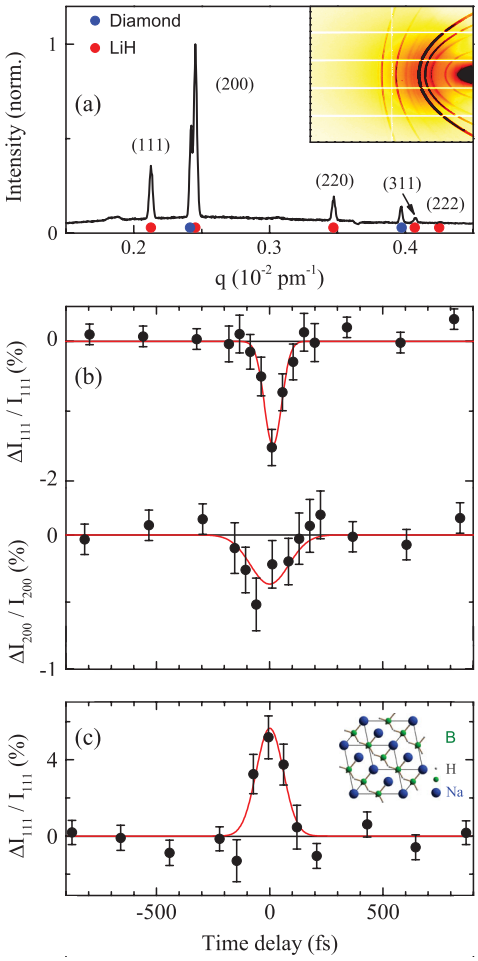

FIG. 1 (color). (a) Diffracted x-ray intensity integrated over individual Debye-Scherrer rings from LiH as a function of the scattering vector $|q|$. Inset: X-ray diffraction pattern as recorded with a large-area x-ray detector. (b) Relative change of diffracted intensity of LiH by the (111) (top) and the (200) (bottom) planes versus the pump-probe time delay. (c) Relative change of the diffracted intensity of $NaBH_4$ by the (111) plane versus time delay. The red lines (Gaussian fits) are guides to the eye.

The LiH and $NaBH_4$ samples consist of a 200 μm thick pressed powder, sealed by two 20 μm thick diamond windows. Considering the ions' shape spherical, both LiH and $NaBH_4$ crystallize in a rock-salt structure (space group $Fm\bar{3}m$) with lattice constants of $a = 407.52$ pm (LiH) [26,27] and $a = 615.06$ pm ($NaBH_4$) [30,31].

The inset of Fig. 1(a) displays part of the detected ring pattern, whereas Fig. 1(a) shows the intensity integrated over the stationary diffraction rings of LiH as a function of the scattering vector q. Two diamond reflections (blue circles) originate from the sample windows. When applying the field of the excitation pulse, we observe the changes of diffracted intensity of all LiH diffraction rings up to (222) while the angular positions remain unchanged. In Fig. 1(b), the change of diffracted intensity on the (111) and (200) rings is plotted as a function of pump-probe delay. One observes a decrease of diffracted intensity of 1%–2% around delay zero, i.e., when excitation and probe pulses interact simultaneously with the sample. The temporal behavior follows essentially the cross correlation between excitation and probe pulses, without any long-lived intensity changes. This fact shows that the induced changes exist only with the excitation field present and that they are fully reversible. The transient intensity change of the (111) reflection of $NaBH_4$ [Fig. 1(c)] is again located around time delay zero but now with a much stronger *positive* amplitude.

The relative intensity change of the diffraction ring hkl is given by

$$\frac{\Delta I_{hkl}(t)}{I_{hkl}} = \frac{|F_{hkl}(t)|^2 - |F^0_{hkl}|^2}{|F^0_{hkl}|^2}, \tag{1}$$

where $F_{hkl}(t)$ is the structure factor of the material modified by the external electric field and F^0_{hkl} the known structure factor of the unexcited crystal. The structure factors are related to the electronic density $\rho(\mathbf{r})$ by a Fourier transform. The steady-state electronic density $\rho_0(\mathbf{r})$ is given by the Fourier transform of the structure factors F^0_{hkl}. In order to account for the limited spatial resolution of our experiment, the structure factors F^0_{hkl} taken from Ref. [27] were multiplied with a Gaussian function $\exp[-\ln(2) \times (q_{hkl}/q_{222})^2]$ to reconstruct the transient electronic density $\rho(\mathbf{r}, t)$ with a spatial resolution compatible with our experiments. For LiH and $NaBH_4$, the structure factors are real due to the inversion symmetry of the rock-salt structure.

Transient electron density maps were derived from the diffraction data with the maximum entropy method (MEM) which has been described in detail elsewhere [32–37]. The stationary structure factors F^0_{hkl} define the initial boundary condition of this iterative procedure, maximizing the so-called entropy which is defined on the basis of charge density. The difference electronic density maps are then computed by $\Delta\rho(\mathbf{r}, t) = \rho(\mathbf{r}, t) - \rho_0(\mathbf{r})$.

In each crystallite of the powder sample, the electric field vector of the excitation pulse $\mathbf{E}(t)$ has an individual

orientation relative to its crystal axes. The transient change of the electron density in an individual crystallite i $[\Delta\rho_i(\mathbf{r}, t) = \rho_i(\mathbf{r}, t) - \rho_0(\mathbf{r})]$ can be decomposed into a symmetry conserving and a nonconserving component $\Delta\rho_i(\mathbf{r}, t) = \Delta\rho^{\mathrm{sym}}(\mathbf{r}, |\mathbf{E}(t)|) + \Delta\rho_i^{\mathrm{nosym}}(\mathbf{r}, \mathbf{E}(t))$. The symmetry conserving part depends only on the amplitude of the electric field $|\mathbf{E}(t)|$ and, thus, is identical in all crystallites; i.e., $\Delta\rho_{\mathrm{sym}}(\mathbf{r}, t)$ exhibits the symmetry properties of the initial structure $\rho_0(\mathbf{r})$. In contrast to our previous study of $LiBH_4$ [25], the present experiments on LiH and $NaBH_4$ did not show any detectable intensity on forbidden reflections. Thus, the symmetry nonconserving component is negligible compared to $\Delta\rho_{\mathrm{sym}}(\mathbf{r}, t)$. The following discussion focuses exclusively on $\Delta\rho_{\mathrm{sym}}(\mathbf{r}, t)$.

The initial electron density map $\rho_0(x, y, 0)$ of LiH is shown in Fig. 2(a) and exhibits a high electron density on the Li atom and a small density on the H atom. In Fig. 2(b), the change of electron density $\Delta\rho_{\mathrm{sym}}(\mathbf{r}, t)$ is plotted for zero delay time. This map shows a pronounced decrease of electron density on the Li atom and a corresponding increase on the hydrogen position, giving direct evidence for a quasi-instantaneous increase of the ionicity of LiH in the presence of the strong electric field. This surprising behavior is in strong contrast to $\Delta\rho_{\mathrm{sym}}(\mathbf{r}, t)$ of $NaBH_4$ shown in Fig. 2(c) and the previously studied $LiBH_4$ [25], where the light-induced charge relocation exhibits an expected charge transfer from the anion (BH_4^-) to the respective cation.

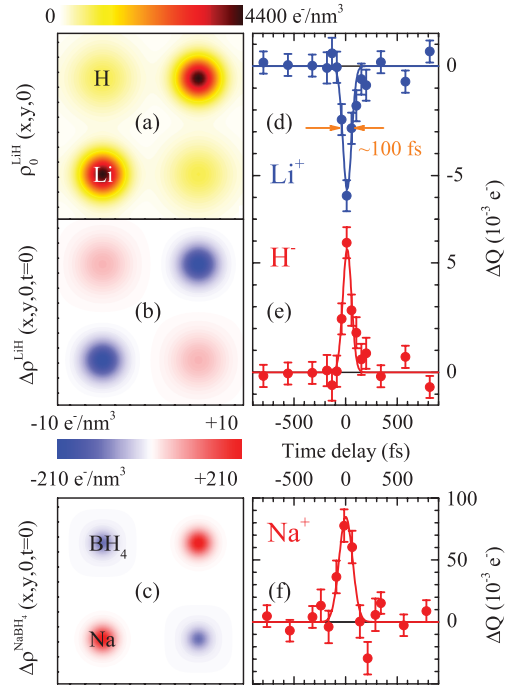

FIG. 2 (color). (a) Stationary electron density distribution of LiH in the $(x, y, 0)$ plane with the spatial resolution of our experiment. (b) Difference electronic density map of LiH reconstructed by the MEM at zero delay time. (c) Difference electronic density map reconstructed by the MEM at the zero delay time of $NaBH_4$. (d),(e) Integrated charge changes of LiH around Li (top) and H (bottom) versus the delay time. (f) Integrated charge changes of $NaBH_4$ around Na^+ versus the delay time.

To determine the amount of charge transferred, we divided the unit cell into subvolumes; i.e., each spatial position $\mathbf{r}$ within the unit cell is uniquely assigned to the subvolume of the nearest atom. We then integrated the charge in the subvolumes. For LiH, this procedure leads to $(a/2)^3$ cubes around Li and H. In the case of BH_4^- anions, the charge of the whole unit was put together. Time-dependent charge density changes are displayed in Figs. 2(d)–2(f). In LiH, the striking feature is a sharp drop of electronic charge on the Li atom [Fig. 2(d)] concomitant with the increase of the same amplitude on the hydrogen position [Fig. 2(e)] around delay zero. The peaks have a width of ≈ 100 fs (FWHM) which agrees with the temporal cross correlation function of the optical excitation and the hard x-ray probe pulses [22,25]. In the case of $NaBH_4$ [Fig. 2(f)], we see exactly the opposite behavior, i.e., a light-induced charge transfer from the anion BH_4^- to the cation Na^+. Outside the temporal overlap of pump and probe pulses, the changes of electron density are minor. Such facts strongly support our picture of a field-driven charge transfer which is limited in time to the presence of the driving field.

We now discuss the microscopic physics underlying the material's polarization and the field-induced change of electron density $\Delta\rho_{\mathrm{sym}}(\mathbf{r}, t)$ in the different materials. Without external field, electrons in an insulator populate states up to the highest valence band. An external field of an amplitude comparable to the interionic field of the order of 1 GV/m distorts the ionic potentials and leads to the admixture of other ionic states, in particular, conduction band states (cf. Fig. 1 of Ref. [25]). The wave function of the mixed state is given by

$$|\Psi_{b,\mathbf{k}}(\mathbf{E})\rangle = \frac{1}{\sqrt{N}}\left[|\Psi_{b,\mathbf{k}}\rangle + \mathbf{E}\sum_{b'\neq b}\frac{\langle\Psi_{b',\mathbf{k}}|e\mathbf{r}|\Psi_{b,\mathbf{k}}\rangle}{\varepsilon_{b,\mathbf{k}} - \varepsilon_{b',\mathbf{k}}}|\Psi_{b',\mathbf{k}}\rangle\right] \tag{2}$$

at wave vector $\mathbf{k}$ in the (occupied) band b with the normalization constant N. The sum runs over all unoccupied bands b'. The perturbative approach in Eq. (2) is valid, as the dipole interaction energy $|\langle\Psi_{b',\mathbf{k}}|e\mathbf{r}|\Psi_{b,\mathbf{k}}\rangle| \cdot |\mathbf{E}| \simeq 0.2$ eV is much smaller than the smallest band gap $\varepsilon_{b,\mathbf{k}} - \varepsilon_{b',\mathbf{k}} \simeq 5$ eV of LiH at the X point of the Brillouin zone. The symmetry conserving part of the deformed charge density is obtained by averaging over all electric field directions ($\hat{\mathbf{e}}_\Omega$ is the unit vector in the solid angle direction Ω) and a summation over all occupied states within the Brillouin zone

$$\rho_{\mathrm{sym}}(\mathbf{r}, t) = \sum_{b,\mathbf{k}}^{\mathrm{occupied}} \frac{1}{4\pi}\int d\Omega |\Psi_{b,\mathbf{k}}(\hat{\mathbf{e}}_\Omega \cdot |\mathbf{E}(t)|, \mathbf{r})|^2. \tag{3}$$

The distorted wave function (2) shows that both the eigenenergies $\varepsilon_{b,\mathbf{k}}$ (i.e., the band structure) and the eigenfunctions $\Psi_{b,\mathbf{k}}(\mathbf{r})$ (i.e., the Bloch functions) of the system Hamiltonian determine the exact shape of the electron density (3) in the strong electric field.

The basis set of wave functions entering into Eq. (2) was determined by quasiparticle calculations within the COHSEX approximation [14] to simultaneously fit the quasiparticle band structure [16] and the stationary electron density [27]. In solving Eq. (1) of Ref. [16], we expanded the quasiparticle band structure in plane waves [38–40] using 339 reciprocal lattice vectors. In contrast to Baroni *et al.* [16], however, we allowed for *inhomogeneous* dielectric screening [41,42] using the dielectric matrix in the space of reciprocal lattice vectors [17]. The latter becomes diagonal for the limiting cases of Baroni *et al.* [16], i.e., $q = 0$ and $q \to \infty$. For intermediate q vectors, the dielectric matrix becomes nondiagonal and we used as fitting parameters two different screening vectors q_s(H) and q_s(Li) for the volumes around the Li^{3+} and H^+ nuclei [43].

Calculations using Eqs. (2) and (3) are summarized in Fig. 3. In the left column, we show (a) the band structure, (b) the valence band electron density ρ_X at the X point where the smallest band gap occurs, (c) the field-induced change of electron density at the X point, and (d) the total change of electron density calculated with Eq. (3). This calculation assumes a homogeneous screening, i.e., $q_s(\mathrm{H})/q_s(\mathrm{Li}) = 1$, as in Ref. [16]. As in mean-field calculations, i.e., Hartree-Fock, the valence band is dominated by 1S-like orbitals on the H atom throughout the Brillouin zone [20]. As a consequence, the stationary electron density corresponds to the fully ionized Li^+ H^- situation. Applying an electric field would reduce the charge on the H^- anion by $\Delta q_H = -0.1e^-$ [Fig. 3(d)], a behavior in striking contrast to our experimental results for LiH [Figs. 2(b) and 2(e)] but close to the behavior of $NaBH_4$ [Figs. 2(c) and 2(f)]. In contrast, Figs. 3(e)–3(h) are calculated with an asymmetric screening vector ratio of $q_s(\mathrm{H})/q_s(\mathrm{Li}) = 2$ [43], resulting in 2P-like valence orbitals on both Li and H nuclei when approaching the valence band at the X point [Fig. 3(f)]. Under the external electric field, the electron density of H^+ increases both at the X point and in total by $\Delta q_H = +0.01e^-$ [Figs. 3(g) and 3(h)], mainly due to admixing 1S-like orbitals now being the dominant contribution to the conduction band at the X point of LiH. This behavior is in *quantitative* agreement with the experiment and reveals the strong impact of an inhomogeneous enhancement of screening at the H^+ site on the wave functions at the X point. To summarize, our calculations show that both the Hartree-Fock mean-field theory and the COHSEX approximation with homogeneous screening [16] wrongly predict a decrease of ionicity of LiH in a strong electric field. Thus, Coulomb correlations among the electrons, being incorporated on the simplest level using COHSEX with inhomogeneous screening, are essential for a field-driven increase of ionicity of LiH as observed in our femtosecond diffraction experiments.

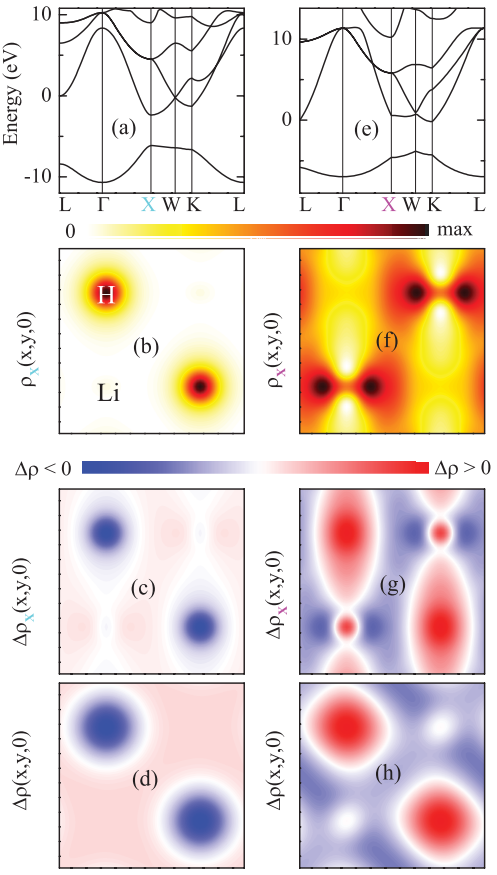

FIG. 3 (color). (a),(e) Quasiparticle band structures of LiH within the COHSEX approximation. (b),(f) Stationary electron densities at the X point. (c),(g) Deformed electron densities at the X point for an external field amplitude $|\mathbf{E}| = 10^9$ V/m. (d), (h) Total density change $\Delta\rho_{\mathrm{sym}}(x, y, 0, t = 0)$ calculated with Eq. (3). The respective charge integrations over $(a/2)^3$ boxes yield (d) $\Delta q_H = -0.1e^-$ and (h) $\Delta q_H = +0.01e^-$. (a)–(d) Calculated with homogeneous screening similar to that of Ref. [16] leading to a 1S-like orbital on the H atom. (e)–(h) Calculated with a somewhat stronger screening on the proton, resulting in 2P-like orbitals on both Li and H nuclei.

In conclusion, spatially resolved electron density maps determined by femtosecond x-ray powder diffraction reveal the prominent role of electron correlations in the response to a nonperturbative external field. In LiH, field-induced correlations between states in the valence and different conduction bands result in an enhancement of ionicity which is manifested in an electron transfer from Li to H and in agreement with band structure calculations. In contrast, $NaBH_4$ display an electron transfer from BH_4^- to Na^+, as expected for an admixture of states in the lowest conduction band. Our results demonstrate the strong potential of femtosecond diffraction methods to uncover microscopic charge dynamics and determine electron transport mechanisms in solids.

This research has received funding from the European Research Council under the European Union's Seventh Framework Programme (FP7/2007-2012)/ERC Grant Agreement No. 247051 and from the Deutsche Forschungsgemeinschaft (Grant No. WO 558/13-1).

*juve@mbi-berlin.de
†Present address: Department of Chemistry and Applied Biosciences, ETH Zürich, Wolfgang-Pauli-Strasse 10, 8093 Zürich, Switzerland.
‡woerner@mbi-berlin.de

[1] W. Kuehn, P. Gaal, K. Reimann, M. Woerner, T. Elsaesser, and R. Hey, Phys. Rev. Lett. **104**, 146602 (2010).
[2] S. Ghimire, A. D. DiChiara, E. Sistrunk, U. B. Szafruga, P. Agostini, L. F. DiMauro, and D. A. Reis, Phys. Rev. Lett. **107**, 167407 (2011).
[3] G. Herink, D. R. Solli, M. Gulde, and C. Ropers, Nature (London) **483**, 190 (2012).
[4] W. Kuehn, P. Gaal, K. Reimann, M. Woerner, T. Elsaesser, and R. Hey, Phys. Rev. B **82**, 075204 (2010).
[5] S. Ghimire, A. D. DiChiara, E. Sistrunk, P. Agostini, L. F. DiMauro, and D. A. Reis, Nat. Phys. **7**, 138 (2011).
[6] T. E. Glover, D. M. Fritz, M. Cammarata, T. K. Allison, S. Coh, J. M. Feldkamp, H. Lemke, D. Zhu, Y. Feng, R. N. Coffee, M. Fuchs, S. Ghimire, J. Chen, S. Shwartz, D. A. Reis, S. E. Harris, and J. B. Hastings, Nature (London) **488**, 603 (2012).
[7] M. Schultze, E. M. Bothschafter, A. Sommer, S. Holzner, W. Schweinberger, M. Fiess, M. Hofstetter, R. Kienberger, V. Apalkov, V. S. Yakovlev, M. I. Stockman, and F. Krausz, Nature (London) **493**, 75 (2013).
[8] A. Schiffrin, T. Paasch-Colberg, N. Karpowicz, V. Apalkov, D. Gerster, S. Mhlbrandt, M. Korbman, J. Reichert, M. Schultze, S. Holzner, J. V. Barth, R. Kienberger, R. Ernstorfer, V. S. Yakovlev, M. I. Stockman, and F. Krausz, Nature (London) **493**, 70 (2013).
[9] D. H. Ewing and F. Seitz, Phys. Rev. **50**, 760 (1936).
[10] W. Kohn, Phys. Rev. **105**, 509 (1957).
[11] R. E. Behringer, Phys. Rev. **113**, 787 (1959).
[12] G. W. Pratt, Jr., Phys. Rev. **118**, 462 (1960).
[13] P. Hohenberg and W. Kohn, Phys. Rev. **136**, B864 (1964).
[14] L. Hedin, Phys. Rev. **139**, A796 (1965).
[15] K.-F. Bergren, J. Phys. C **2**, 802 (1969).
[16] S. Baroni, G. Pastori Parravicini, and G. Pezzica, Phys. Rev. B **32**, 4077 (1985).
[17] M. S. Hybertsen and S. G. Louie, Phys. Rev. B **34**, 5390 (1986).
[18] L. Bellaiche, J. M. Besson, K. Kunc, and B. Lévy, Phys. Rev. Lett. **80**, 5576 (1998).
[19] S. Lebégue, M. Alouani, B. Arnaud, and W. E. Pickett, Europhys. Lett. **63**, 562 (2003).
[20] N. Novakovic, I. Radisavljevic, D. Colognesi, S. Ostojic, and N. Ivanovic, J. Phys. Condens. Matter **19**, 406211 (2007).
[21] M. Bargheer, N. Zhavoronkov, Y. Gritsai, J. C. Woo, D. S. Kim, M. Woerner, and T. Elsaesser, Science **306**, 1771 (2004).
[22] M. Woerner, F. Zamponi, Z. Ansari, J. Dreyer, B. Freyer, M. Prémont-Schwarz, and T. Elsaesser, J. Chem. Phys. **133**, 064509 (2010).
[23] F. Zamponi, P. Rothhardt, J. Stingl, M. Woerner, and T. Elsaesser, Proc. Natl. Acad. Sci. U.S.A. **109**, 5207 (2012).
[24] B. Freyer, F. Zamponi, V. Juv, J. Stingl, M. Woerner, T. Elsaesser, and M. Chergui, J. Chem. Phys. **138**, 144504 (2013).
[25] J. Stingl, F. Zamponi, B. Freyer, M. Woerner, T. Elsaesser, and A. Borgschulte, Phys. Rev. Lett. **109**, 147402 (2012).
[26] R. S. Calder, W. Cochran, D. Griffiths, and R. D. Lowde, J. Phys. Chem. Solids **23**, 621 (1962).
[27] G. Vidal-Valat and J.-P. Vidal, Acta Crystallogr. Sect. A **48**, 46 (1992).
[28] F. Zamponi, Z. Ansari, M. Woerner, and T. Elsaesser, Opt. Express **18**, 947 (2010).
[29] N. Zhavoronkov, Y. Gritsai, M. Bargheer, M. Woerner, Th. Elsaesser, F. Zamponi, I. Uschmann, and E. Förster, Opt. Lett. **30**, 1737 (2005).
[30] P. Fischer and A. Züttel, Mater. Sci. Forum **443–444**, 287 (2004).
[31] R. S. Kumar and A. L. Cornelius, Appl. Phys. Lett. **87**, 261916 (2005).
[32] E. T. Jaynes, Phys. Rev. **106**, 620 (1957).
[33] C. J. Gilmore, Acta Crystallogr. Sect. A **52**, 561 (1996).
[34] S. Yamamura, S. Kasahara, M. Takata, Y. Sugawara, and M. Sakata, J. Phys. Chem. Solids **60**, 1721 (1999).
[35] S. van Smaalen, L. Palatinus, and M. Schneider, Acta Crystallogr. Sect. A **59**, 459 (2003).
[36] L. Palatinus and S. van Smaalen, Acta Crystallogr. Sect. A **61**, 363 (2005).
[37] In our data analysis, we used the MEM [32,33] as implemented in the BayMEM software [35].
[38] M. L. Cohen, P. J. Lin, D. M. Roessler, and W. C. Walker, Phys. Rev. **155**, 992 (1967).
[39] J. R. Chelikowsky and M. L. Cohen, Phys. Rev. B **14**, 556 (1976).
[40] I. Ohkoshi, J. Phys. C **18**, 5415 (1985).
[41] N. Wiser, Phys. Rev. **129**, 62 (1963).
[42] A. Baldereschi and E. Tosatti, Solid State Commun. **29**, 131 (1979).
[43] Details of our COHSEX calculation [14], which is based on a plane wave approach [40] including inhomogeneous dielectric screening [41,42], will be published elsewhere.